Supplementary material for "The sensitivity of lowermost mantle anisotropy to past mantle convection"

James Ward[a,1], Andrew M. Walker[b], Andy Nowacki[a,*], James Panton[c], J. Huw Davies[c]

[a]*School of Earth and Environment, University of Leeds, Leeds, LS2 9JT, West Yorkshire, United Kingdom*
[b]*Department of Earth Sciences, University of Oxford, Oxford, OX1 3AN, Oxfordshire, United Kingdom*
[c]*School of Earth and Environmental Sciences, Cardiff University, Cardiff, CF10 3AT, Cardiff, United Kingdom*

1. Supplementary figures

In this supplementary material we include additional figures showing radial P-wave anisotropy for all ease-of-texture cases (Figure S1), comparisons between radial anisotropy for the two flow models (Figs. S2–S7) and cumulative histograms of radial anisotropy values (Figs. S8 and S9).

*Corresponding author: a.nowacki@leeds.ac.uk
[1]Now at HM Government Statistical Service
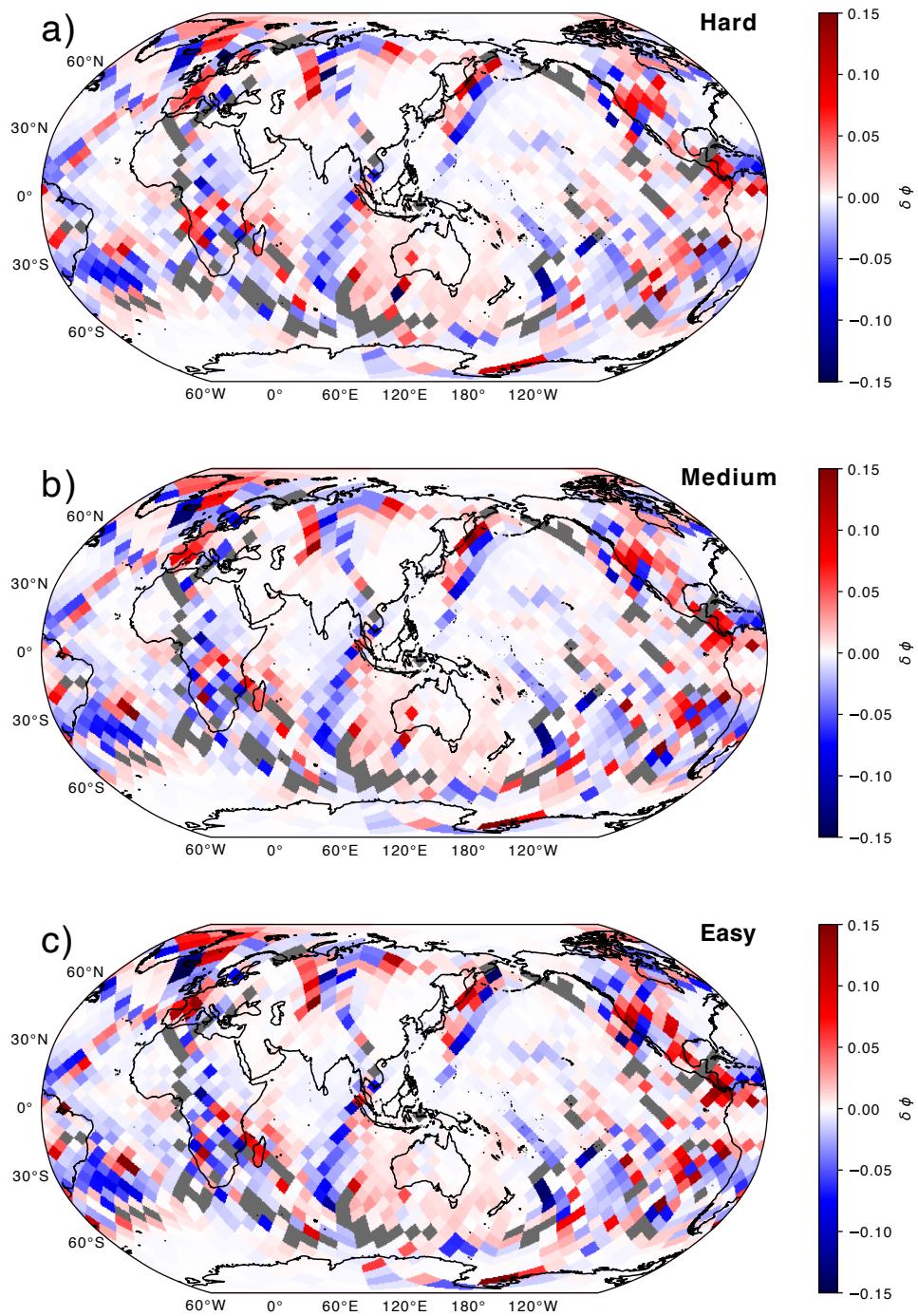
Figure S1: Maps showing the difference between P-wave radial anisotropy (ϕ) at 3530 km radius (50 km above the core–mantle boundary) for the different flow fields with the different ease-of-texturing cases. The regions in grey show where post-perovskite is not predicted to be stable at this depth.
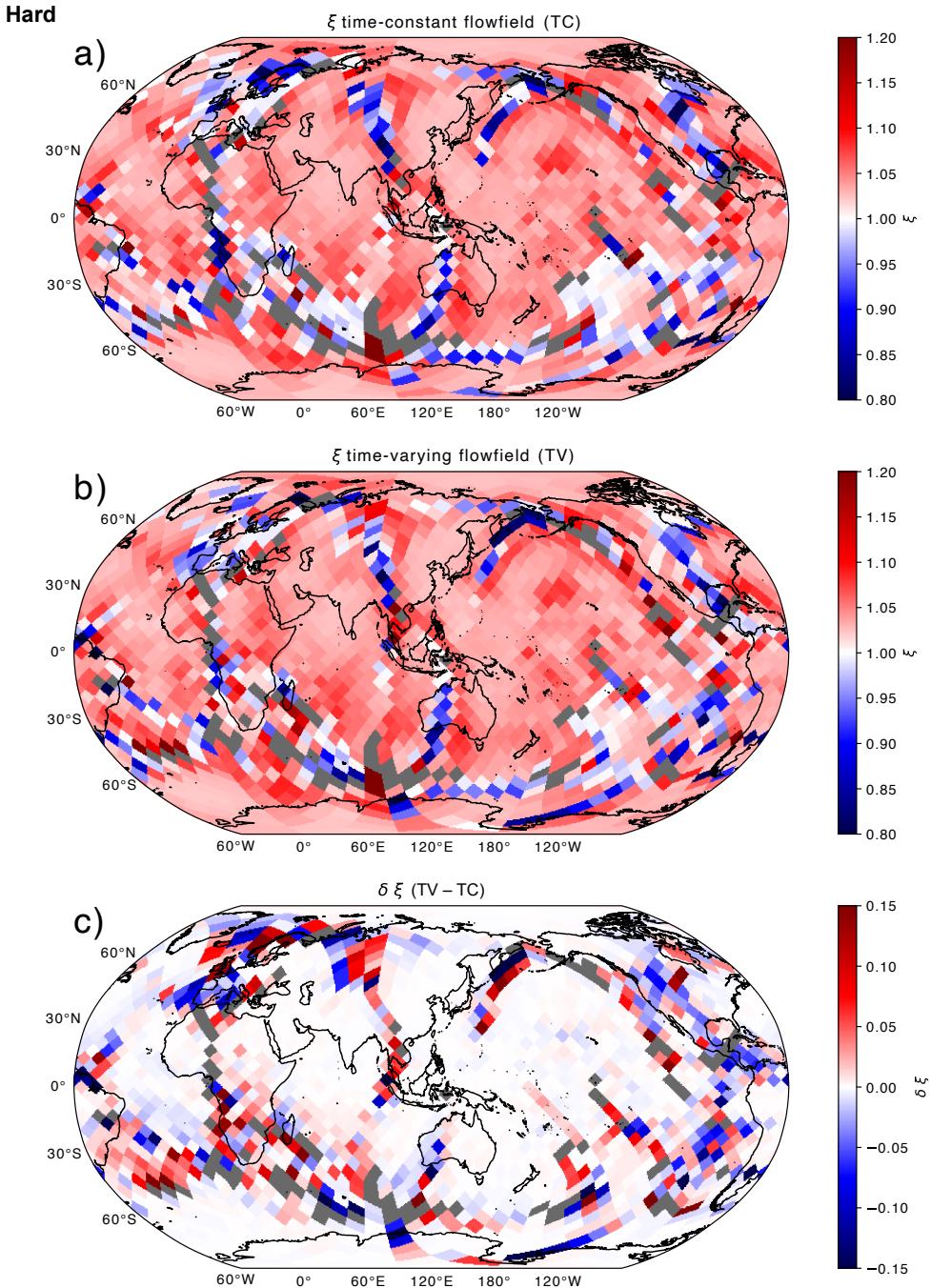
Figure S2: Maps of S-wave radial anisotropy (ξ) at 3530 km radius (50 km above the core–mantle boundary) for the *hard-to-texture case*. We show ξ calculated with the time-constant (TC) flowfield (a), the time-varying (TV) flowfield (b) and the difference between the two (c).
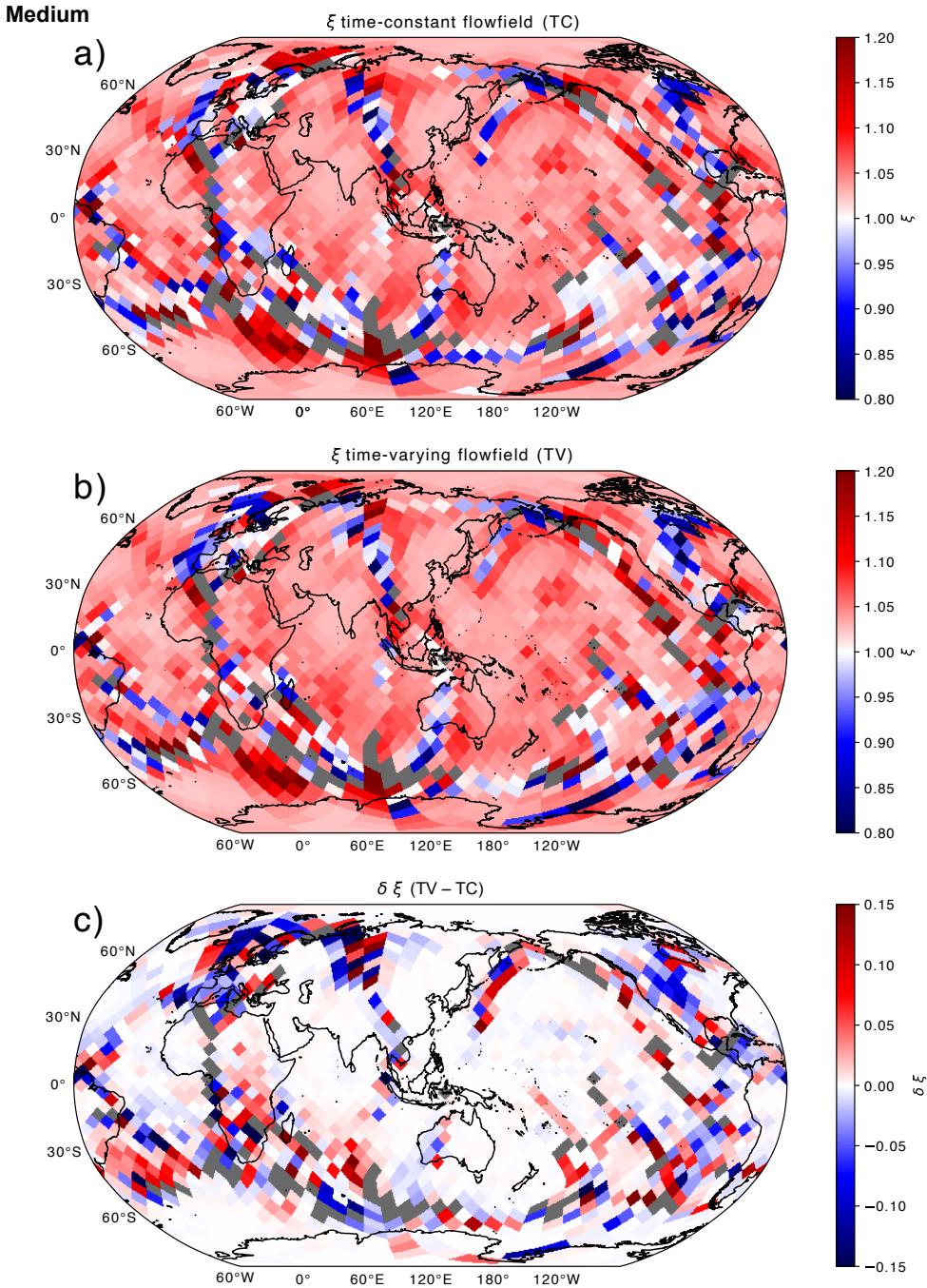
Figure S3: Maps of S-wave radial anisotropy (ξ) at 3530 km radius (50 km above the core–mantle boundary) for the *medium texture case*. We show ξ calculated with the time-constant (TC) flowfield (a), the time-varying (TV) flowfield (b) and the difference between the two (c).
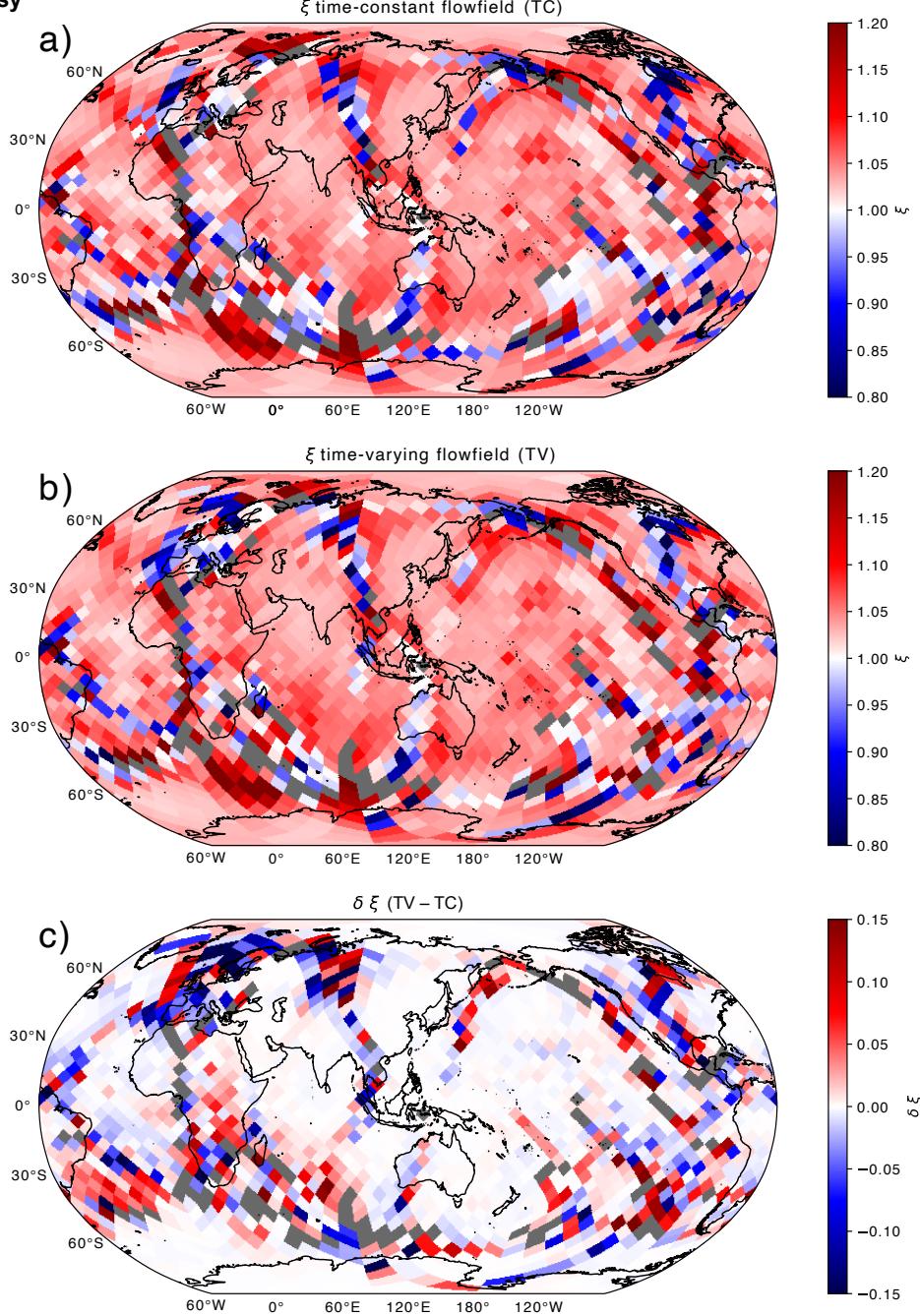
Figure S4: Maps of S-wave radial anisotropy (ξ) at 3530 km radius (50 km above the core–mantle boundary) for the *easy-to-texture case*. We show ξ calculated with the time-constant (TC) flowfield (a), the time-varying (TV) flowfield (b) and the difference between the two (c).
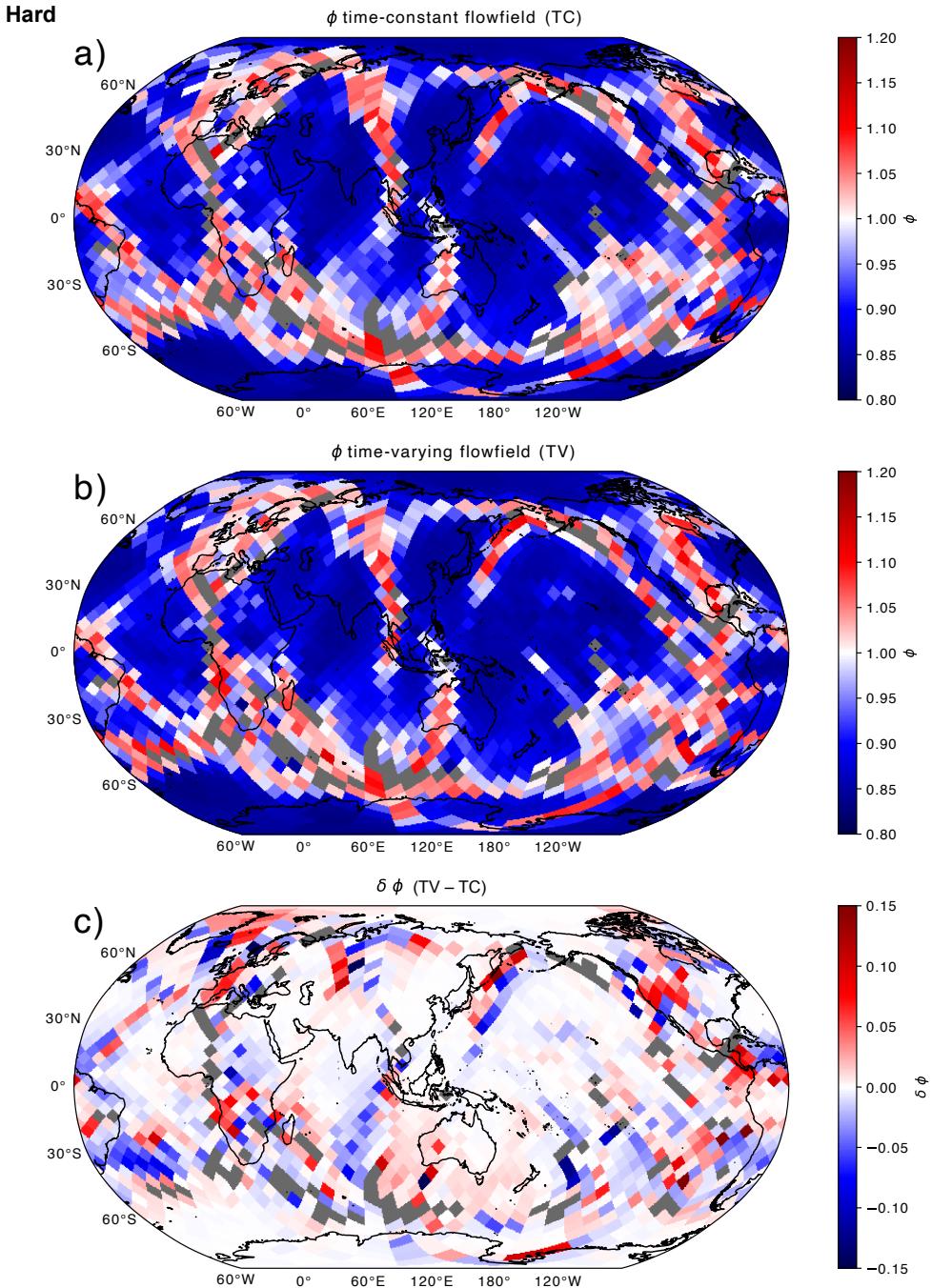
Figure S5: Maps of P-wave radial anisotropy (ϕ) at 3530 km radius (50 km above the core–mantle boundary) for the *hard-to-texture case*. We show ϕ calculated with the time-constant (TC) flowfield (a), the time-varying (TV) flowfield (b) and the difference between the two (c).
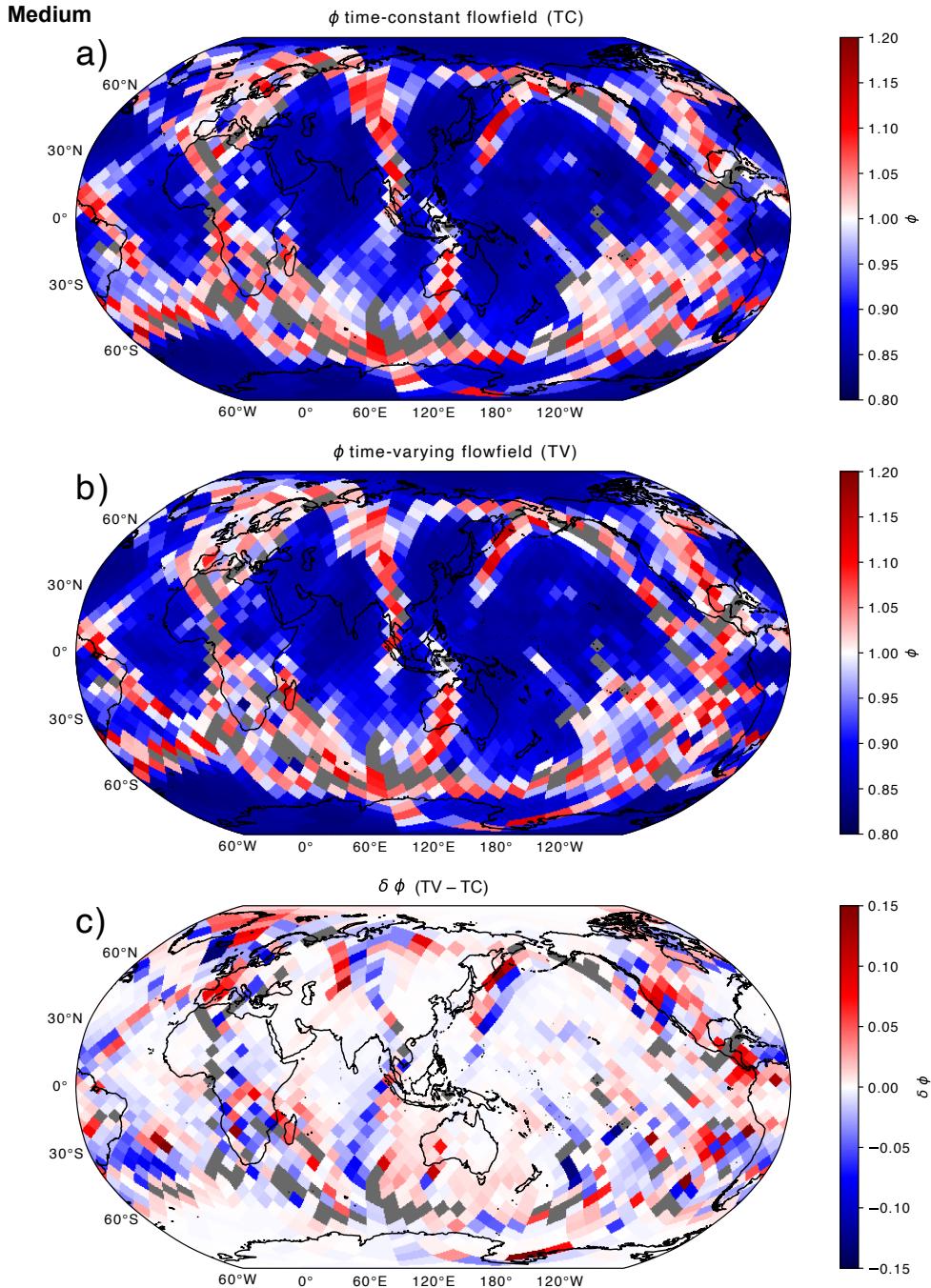
Figure S6: Maps of P-wave radial anisotropy (ϕ) at 3530 km radius (50 km above the core–mantle boundary) for the *medium texture case*. We show ϕ calculated with the time-constant (TC) flowfield (a), the time-varying (TV) flowfield (b) and the difference between the two (c).
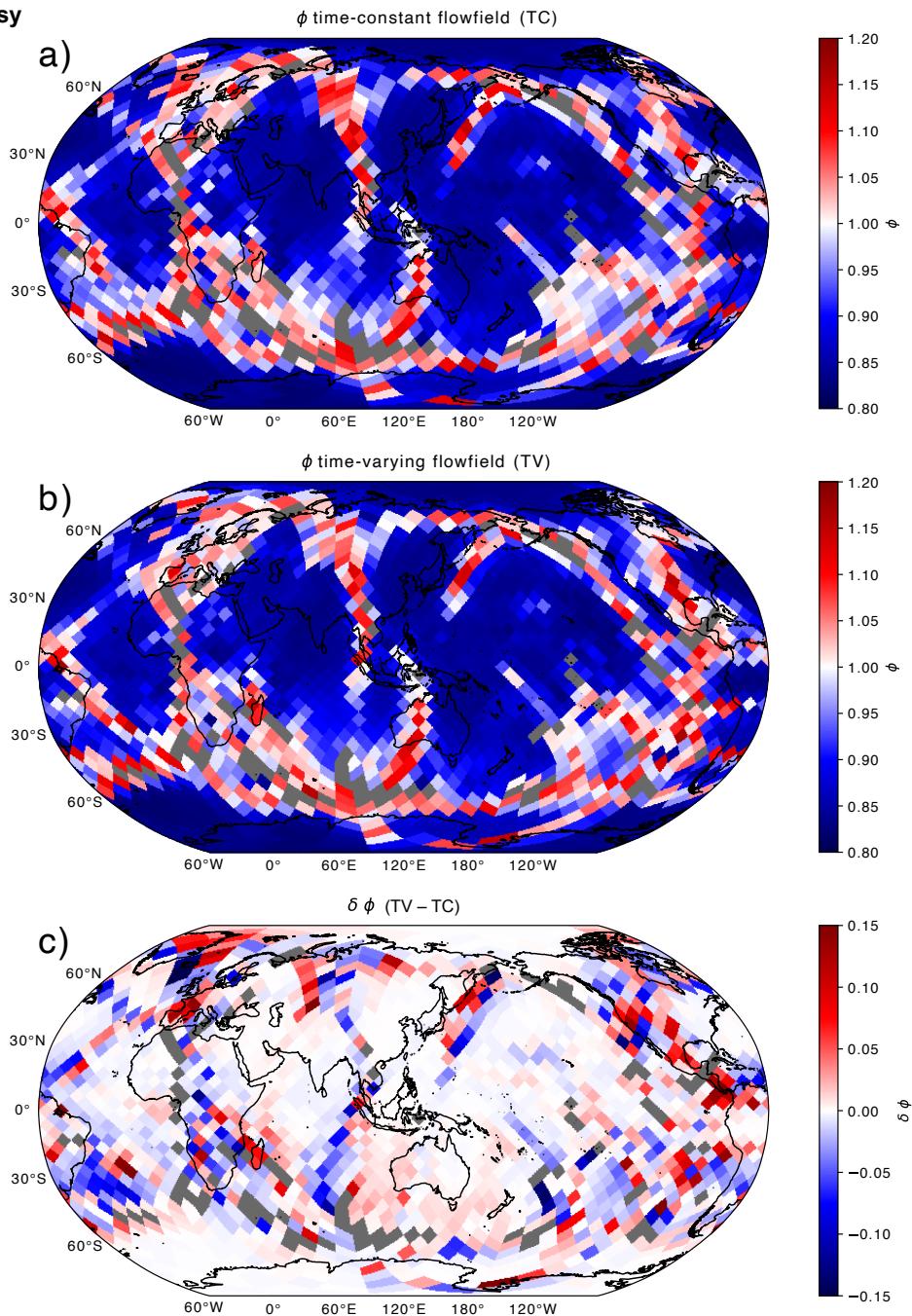
Figure S7: Maps of P-wave radial anisotropy (ϕ) at 3530 km radius (50 km above the core–mantle boundary) for the *easy-to-texture case*. We show ϕ calculated with the time-constant (TC) flowfield (a), the time-varying (TV) flowfield (b) and the difference between the two (c).
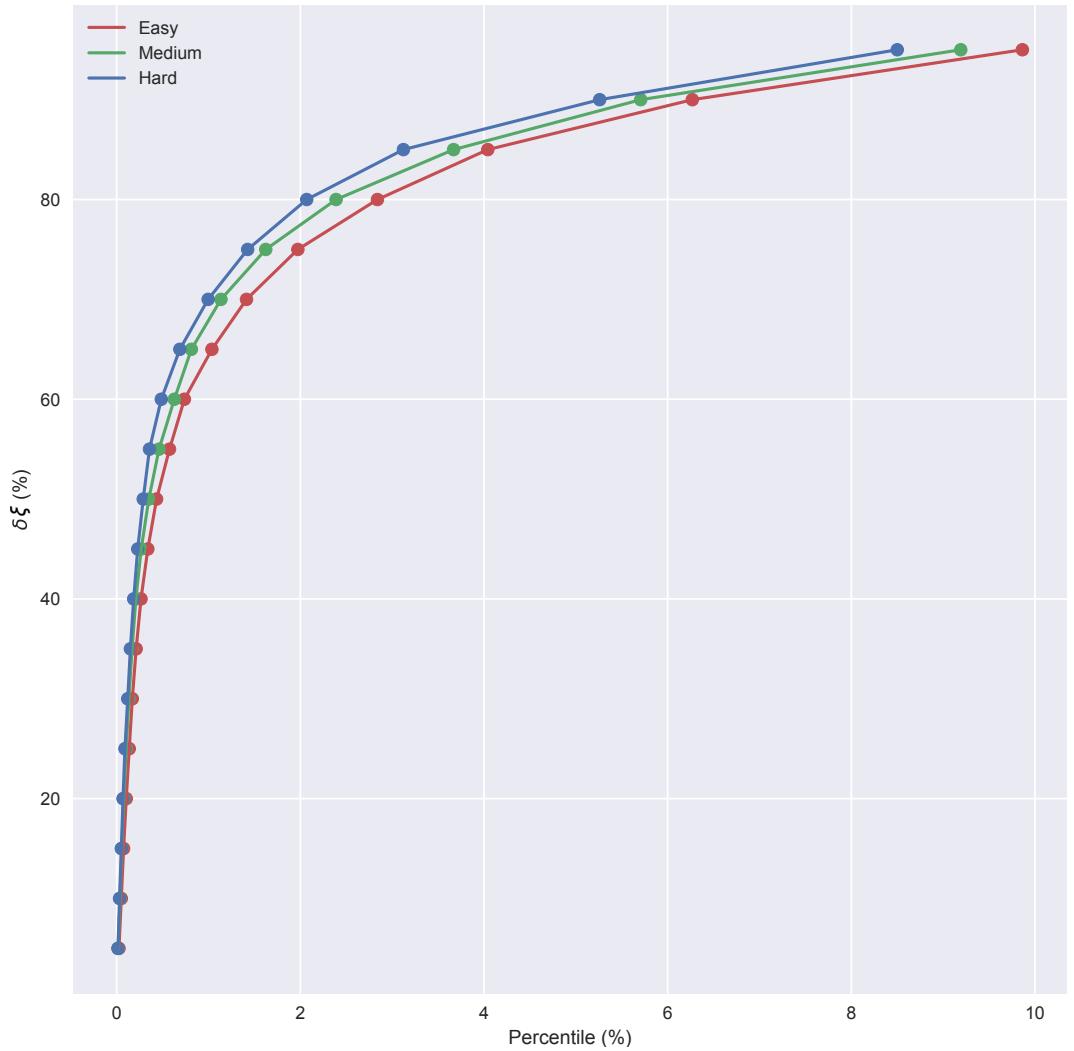
Figure S8: Cumulative histograms showing the effect of slip system activities on the sensitivity of ξ observations to past flow in the lower mantle. This figure shows the different percentile ξ values coloured by the slip system label from Table 2 (main text). Notice at the larger percentiles the easy-to-texture case always has larger differences in ξ between the flow fields.
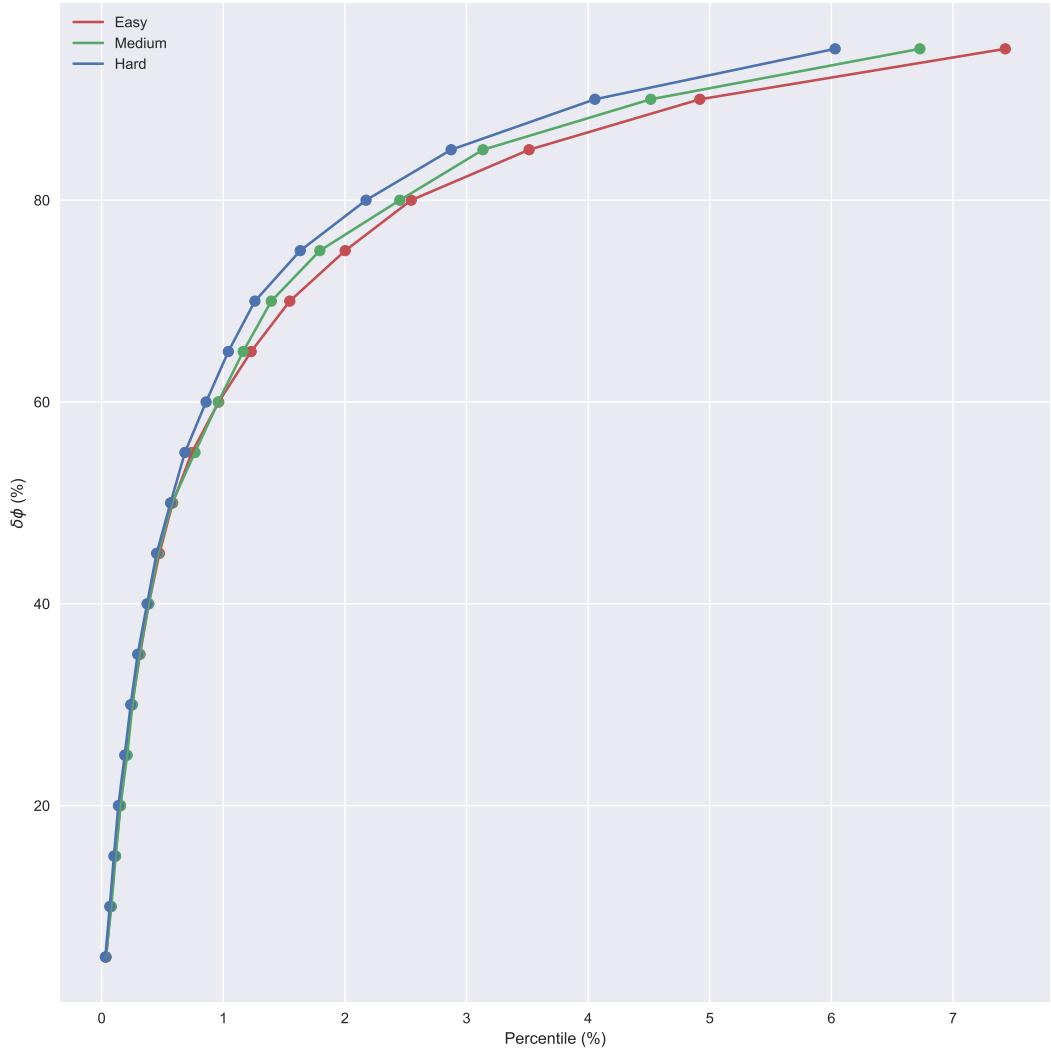
Figure S9: Cumulative histograms showing the effect of slip system activities on the sensitivity of ϕ observations to past flow in the lower mantle. This figure shows the different percentile ϕ values coloured by the slip system label from Table 2 (main text). Notice at the larger percentiles the easy-to-texture case always has larger differences in ϕ between the flow fields.